HHS Public Access

Author manuscript

Bone. Author manuscript; available in PMC 2023 January 01.

Published in final edited form as:

Bone. 2022 January ; 154: 116201. doi:10.1016/j.bone.2021.116201.

Sclerostin antibody improves phosphate metabolism hormones, bone formation rates, and bone mass in adult *Hyp* mice

Kelsey A. Carpenter[1], **Reid Davison**[1], **Shruti Shakthivel**[1], **Kyle D. Anderson**[1], **Frank C. Ko**[1,2], **Ryan D. Ross**[1,2]

[1]Department of Cell & Molecular Medicine, Rush University Medical Center, Chicago, IL

[2]Department of Orthopedic Surgery, Rush University Medical Center, Chicago, IL

Abstract

X-linked hypophosphatemia (XLH) is caused by a loss-of-function mutation in the phosphate regulating gene with homology to endopeptidase located on the X chromosome (PHEX). Loss of functional PHEX results in elevated fibroblast growth factor 23 (FGF23), impaired phosphate reabsorption, and inhibited skeletal mineralization. Sclerostin, a protein produced primarily by osteocytes, suppresses bone formation by antagonizing canonical Wnt-signaling and is reported to be elevated in XLH patients. Our previous study reported that a monoclonal antibody to sclerostin (Scl-Ab) decreases FGF23 and increases phosphate and bone mass in growing *Hyp* mice (XLH murine model). In the current study, we investigated the efficacy of Scl-Ab in treating XLH pathophysiology in adult *Hyp* mice that are past the period of rapid skeletal growth (12 and 20-weeks old). We hypothesized that Scl-Ab would not only increase bone formation, bone strength and bone mass, but would also normalize phosphate regulating hormones, FGF23, parathyroid hormone (PTH), and vitamin 1,25(OH)2D. Scl-Ab treatment increased cortical area, trabecular bone volume fraction, trabecular bone formation rate, and the bending moment in both sexes of both age groups. Scl-Ab treatment suppressed circulating levels of intact FGF23 and c-term FGF23 in treated male and female wild-type and *Hyp* mice of both age groups and improved both vitamin 1,25(OH)2D and PTH. Scl-Ab treated *Hyp* mice also showed evidence of increased renal expression of the sodium-phosphate co-transporter, NPT2a, specifically in the female *Hyp* mice. Our study suggests that Scl-Ab treatment can improve several skeletal and metabolic pathologies associated with XLH, further establishes the role of sclerostin in the regulation of FGF23 and provides evidence that Scl-Ab can improve phosphate regulation by targeting the bone-renal axis.

CRediT Authorship Contribution Statement

Kelsey A. Carpenter: Conceptualization, Investigation, Formal Analysis, Visualization, Writing – Original draft, Writing – Review & Editing. **Reid Davison:** Investigation, Writing – Review & Editing. **Shruti Shakthivel:** Investigation, Writing – Review & Editing **Kyle D. Anderson:** Investigation, Writing – Review & Editing. **Frank C. Ko:** Investigation, Writing – Review & Editing. **Ryan D. Ross:** Conceptualization, Writing – Original draft, Writing – Review & Editing, Funding Acquisition, Supervision, Project Administration. All authors approved the final version of the manuscript.

Keywords

XLH; FGF23; Sclerostin; Mineral Metabolism

Introduction

X-linked Hypophosphatemia (XLH) is the most common form of inherited rickets [1]. XLH is caused by inactivating mutations in the phosphate regulating neutral endopeptidase on the X-chromosome (PHEX) [2]. Inactivating PHEX mutations result in elevated fibroblast growth factor 23 (FGF23) production, which impairs renal phosphate reabsorption through suppression of sodium-phosphate transporters (Npt2a/2c), leading to hypophosphatemia, or low circulating phosphate levels. Clinically, the combination of hypophosphatemia and the accumulation of mineralization inhibitors within the bone tissue results in osteoid accumulation, decreased bone mineral density, and increased fracture risk [3].

Phosphate is regulated as part of a multi-organ endocrine loop, involving FGF23, parathyroid hormone (PTH), and active vitamin D (1,25(OH)2D) [4]. Importantly, these hormones also influence the expression of one another [5]. For example, in addition to suppressing renal phosphate reabsorption, FGF23 also reduces 1,25(OH)2D production by inhibiting the renal expression of Cyp27B1 (encoding for a hydroxylase which activates 1,25(OH)2D) and increasing the expression of Cyp24A1 (encoding for a hydroxylase which inactivates 1,25(OH)2D). Low 1,25(OH)2D levels are commonly noted in patients with XLH [6]. FGF23 can also suppress PTH production [7–9], yet patients with XLH are commonly reported to have abnormally high levels of PTH [10]. Therefore, the combined activity of high FGF23, low 1,25(OH)2D, and elevated PTH contribute to reduced circulating phosphate and the resulting skeletal pathologies in XLH.

Our laboratory has recently demonstrated that sclerostin antibody (Scl-Ab) treatment decreases the circulating levels of FGF23 in the *Hyp* mouse model of XLH [11], demonstrating a role for sclerostin in phosphate metabolism. Consistent with our findings, FGF23 levels are lower in the sclerostin null mouse [12] and treatment of cultured osteocyte-like (IDG-SW3) cells with sclerostin upregulates FGF23 expression [13]. Loss of sclerostin, such as in the sclerostin null mice leads to increased circulating 1,25(OH)2D, which may be due to direct effects of sclerostin on the renal expression of Cyp27b1 [12]. These findings, combined with the well-established regulation of sclerostin expression by PTH [14], led us to hypothesize that in addition to reducing circulating FGF23, Scl-Ab treatment would improve 1,25(OH)2D and PTH levels in *Hyp* mice. To test this hypothesis, we investigated the global effects of Scl-Ab on phosphate regulating hormones and the bone-renal axis. Our results show that Scl-Ab treatment decreased FGF23 and PTH levels and mildly increased 1,25(OH)2D. Further, we also found evidence that Scl-Ab increases the renal protein expression of the sodium-phosphate co-transporter, NPT2a in female *Hyp* mice.

Materials and Methods

Animals

Female heterozygous (+/*Hyp*) [000528] and male wild-type C57BL/6 (WT; +/y) mice were purchased from Jackson Laboratory (Bar Harbor, ME, USA). The breeding strategy generated heterozygous (+/*Hyp*) and WT females and hemizygous (*Hyp*/y) and WT males. Mice were weaned at 4 weeks of age, caged in groups of 3 to 5, maintained on a 12-hour dark/light cycle, and were provided standard Teklad Global 18% protein rodent chow (2018, Teklad, Madison, WI, USA; 1% Ca, 0.7% phosphorus) and water *ad libitum*. Two age groups were used for this study, 12-week-old mice and 20-week-old mice. All mice were randomly assigned to twice weekly subcutaneous injections of either 25 mg/kg Scl-Ab (Amgen Inc, Thousand Oaks, CA and UCB Pharma, Brussels, Belgium) or vehicle (saline). The 12-week-old cohort received treatment beginning at 4 weeks of age and continued for 8 weeks, until sacrifice at 12 weeks of age. The 20-week-old cohort received treatment beginning at 12 weeks of age for 8 weeks, until sacrifice at 20 weeks of age. The treatment strategy was designed to capture mice as they approached the end of longitudinal bone growth [15] and to be similar to that used by Ren et al. in the autosomal recessive hypophosphatemic rickets (ARDR) model [16]. Mice from both age groups were given subcutaneous injections of calcein (12 mg/kg) to label mineralizing bone at 7 and 2 days before sacrifice. Sample sizes for the 12-week-old cohort ranged between 5–8 mice and sample sizes for the 20-week-old cohort ranged between 10–15 mice. All animal studies were approved by the Rush University Institutional Animal Care and Use Committee.

Animals were sacrificed 24-hours after the last treatment injection. Body mass was measured immediately after sacrifice. Blood was collected via cardiac puncture into serum collection tubes (BD Microtainer #365978) and allowed to clot at room temperature for 30 minutes before being centrifuged at 6,000 rcf for 90 sec at 4°C to separate serum. Right femurs were collected, stored in 70% ethanol at 4°C. Left femurs were fresh-frozen at −20°C. Kidneys from the 12-week-old mice were stored in RNAlater and frozen at −20°C. Left kidneys from the 20-week-old mice were fixed in 10% neutral buffered formalin for 48 hours and subsequently stored in 70% ethanol.

Circulating factors

Serum phosphate and serum calcium levels were measured in both age groups using colorimetric assays (Pointe Scientific). Urine phosphate and urine creatinine were measured in the 20-week-old cohort using colorimetric assays (Pointe Scientific). Serum PTH (Quidel), intact FGF23 (Quidel), c-term FGF23 (Quidel), and 1,25(OH)2D (Immunodiagnostic systems) were measured in both age groups using enzyme-linked immunosorbent assay (ELISA).

Micro-computed tomography

Right femurs of both age groups were micro-computed tomography (μCT) scanned while submerged in 70% ethanol, perpendicular to the long axis. Scanning parameters were 55 kVp and 145 μA, with a 500 ms integration time and a 6 μm isotropic voxel size (μCT50, Scanco Medical). Length of each femur was measured from the most proximal slice of the

femur to the most distal slice. Cortical geometry was measured in the middle 100 slices of the femoral diaphysis. Primary cortical parameters included cortical area (Ct.Ar), total area (Tt.Ar), medullary area (Ma.Ar), cortical thickness (Ct.Th), and cortical porosity (Ct.Po). Trabecular bone architecture was measured from the distal 30% slice of the total femoral length to the distal growth plate. Primary trabecular parameters included bone volume per total volume (BV/TV), trabecular number (Tb.N), trabecular thickness (Tb.Th), and trabecular spacing (Tb.S). All parameters are reported using conventional nomenclature [17].

Mechanical Testing

Left femurs of both age groups were thawed in phosphate-buffered saline prior to 3-point bending. Femurs were loaded to failure in the anterior-posterior direction, with the tensile surface on the posterior side of the femur. A lower support span length of 7 mm was used for WT mice and 5 mm for *Hyp* mice, approximating ~65% of the average femoral length for both genotypes. Data was collected using a load rate of 0.1 mm/s and a data acquisition rate of 100 Hz (MTS CriterionTM). A preload of ~0.5 N was applied to each bone to prevent shifting during testing. Load-displacement curves were used to determine maximum load and stiffness. The maximum load and the stiffness were then converted to bending moment and bending rigidity, respectively, to account for the differences in span length used for the WT and Hyp tissues [18].

Skeletal Histology

Following μCT scanning, the right femur was dehydrated in a series of graded alcohol solutions and then embedded in polymethyl methacrylate (PMMA). Longitudinal sections were cut in the coronal plane to a 5 μm thickness and mounted onto glass slides. Using embedded calcein labels, one section from each mouse was analyzed for endocortical and trabecular bone formation parameters including mineralizing surface (MS/BS; %), mineral apposition rate (MAR; μm/d), and bone formation rate (BFR/BS; μm3/μm2/day). Trabecular bone dynamics were measured in the medullary cavity in a region of interest that started just proximal to the growth plate and continued 1.5 mm proximally along the length of the bone and included all medullary space between the endocortical surfaces. Conventional dynamic histomorphometric protocols were used [19]. Cortical bone dynamics were measured on the endocortical surface in a region of interest that began where the trabecular region of interest ended and continued 1.5 mm proximally. Both medial and lateral endocortical surfaces were evaluated. If no double calcein label was present, an imputed MAR value of 0.3 was used to calculate BFR.

Following bone formation analyses, slides were stained with Goldner's trichrome bone stain. Cortical and trabecular osteoid surface was evaluated using Osteomeasure (osteometrics) in the same region of interest as was used for bone formation analyses. Primary outcome measures included cortical and trabecular osteoid width (O.Wi) and osteoid surface/bone surface (OS/BS). Trabecular and endocortical mineralization lag time (Tb.MLT and Ec.MLT) were determined as the O.Wi divided by the MAR. If O.Wi was not present, MLT was recorded as undetected.

Gene Expression

Kidneys from 12-week-old mice were thawed, snap frozen in liquid nitrogen, and subsequently crushed with a mortar and pestle. The crushed contents were then submerged in Trizol (Ambion) and homogenized with a Polytron PT 10–35 Homogenizer (Brinkmann). RNA was extracted using the manufacturer's protocol (Trizol) and purified using an RNA purification kit (MidSci #IB47302) before being reverse transcribed using an Applied Biosystems High capacity cDNA Reverse Transcription Kit. qPCR (QuantStudioTM 7 Flex System using SYBR Green reagents) was completed to detect gene expression of sodium-phosphate transporters (NaPt2a and Napt2c). Gapdh was used as the internal control. GAPDH-F 5' AGG TCG GTG TGA ACG GAT TTG 3' GAPDH-R 5' GGG GTC GTT GAT GGC AAC A 3'; NPT2a-F 5' CTC ATT GGC CTG GGT GTG AT 3' NPT2a-R 5'AGC GGG TAC CAC AGT AGG AT 3'; NPT2c-F 5' CAG AGC TAG GAT TGG GCC TG 3' NPT2c-R 5' TCC AGC CAT TTT GCT GCC TA 3'.

Immunohistochemistry

Left kidneys from 20-week-old mice were paraffin embedded, sectioned at 5 μm thickness, and immunostained for NPT2a. Briefly, sample sections were de-paraffinized, rehydrated and antigen unmasking was performed by incubating samples in Trypsin (Sigma T7168) at 37°C for 30 min. The slides were then washed with tris-buffered saline three times followed by blocking in 3% H_2O_2 for 10 min at room temperature. Samples were incubated at 4°C overnight in primary antibody for NPT2a (Invitrogen, SLC34A1 Antibody PA5-113005) at a 1:200 dilution. AntiRabbit biotinylated secondary antibody was applied to the samples at a 1:300 dilution for 30 min at room temperature. A Tyramide Signal Amplification kit (Perkin Elmer #NEL700A) was used to amplify the binding signal followed by a DAB Peroxidase Substrate Kit (Vector SK-4100). Thionin (0.1%) was used as a counterstain for 10 seconds.

Statistical Analyses

Variables were compared separately for males and females using a two-way analysis of variance (ANOVA) with genotype and treatment as the independent factors. When significant genotype by treatment interactions were noted, post-hoc analysis was performed using an independent student's t-test. Undetected variables were set to 0.3 in the case of MAR or 0 in the case of MLT. A p-value of <0.05 was considered statistically significant.

Results

Mineral Metabolism Markers

Serum intact FGF23 (iFGF23) was significantly elevated in *Hyp* mice of both sexes and age groups (Figure 1A and Figure 2A). Scl-Ab treatment decreased iFGF23 in all groups, although the effects were not significant in male mice in the 12-week age group (Treatment effect: p=0.073). The 12-week female, 20-week male, and 20- week female groups had significant genotype x treatment interactions for iFGF23, with *Hyp* mice responding to Scl-Ab with a greater decrease in iFGF23 when compared to WT mice (12-week females: 30% WT, 51% *Hyp*; 20-week males: 21% WT, 73% *Hyp*; 20-week females: 23% WT, 26% *Hyp*).

Serum c-term FGF23 (cFGF23) was similarly elevated in *Hyp* mice of both sexes and age groups (Figure 1B and Figure 2B). Scl-Ab significantly decreased circulating cFGF23 in both sexes and age groups. The 12-week male, 12-week female, and 20-week female groups had significant genotype x treatment interactions for cFGF23, with *Hyp* mice responding to Scl-Ab with a greater decrease in cFGF23 when compared to WT mice (12-week males: 13% WT, 35% *Hyp*; 12-week females: 5% WT, 54% *Hyp*; 20-week females: 12% WT, 33% *Hyp*).

Circulating phosphate levels were not different in *Hyp* mice when compared to WTs. Scl-Ab increased circulating phosphate levels in female in the 12-week age group, but there were no Scl-Ab treatment effects in any other cohort (Figure 1C and Figure 2C). Circulating calcium levels were not different in *Hyp* mice when compared to WTs. Scl-Ab treatment did not affect calcium levels in any sex or age groups (Figure 1D and Figure 2D). Circulating vitamin 1,25(OH)2D levels were elevated in female *Hyp* mice of the 20-week age group, but there were no genotype effects in any other cohort. Scl-Ab increased 1,25(OH)2D in both sexes of the 20-week age group, but not in the 12-week age group (Figure 1E and Figure 2E). Serum PTH levels were not different in *Hyp* mice compared to WTs. Scl-Ab treatment decreased PTH in male mice in the 20-week group only (Figure 1F and Figure 2F).

Urine phosphate/urine creatinine ratios did not differ in *Hyp* mice compared to WTs in either sex. Scl-Ab treatment had no effect on urine phosphate/urine creatinine ratios (Supplemental Tables 1 & 2).

Micro-computed Tomography (μCT)

Femurs of *Hyp* mice were significantly shorter than WTs with no improvements in femoral length observed with Scl-Ab treatment (data not shown). *Hyp* mice in both sexes and age groups had decreased cortical area (Ct.Ar) compared to WTs (Figure 3A and Figure 3B). Scl-Ab treatment increased cortical area in all groups. The 20-week male and 20-week female groups had significant genotype x treatment interactions for cortical area, with WT mice responded to Scl-Ab with a greater increase in cortical area when compared to *Hyp* mice (20-week males: 32% WT, 28% *Hyp*; 20-week females: 43% WT, 23% *Hyp*).

Total area (Tt.Ar) did not differ between *Hyp* and WT mice. Scl-Ab treatment increased Tt.Ar in both sexes of both age groups. *Hyp* mice had increased medullary area (Ma.Ar) compared to WTs in both sexes and age groups. Interestingly, the effects of Scl-Ab treatment on Ma.Ar appear to be age, sex, and genotype dependent, as Scl-Ab led to increased Ma.Ar in 12-week *Hyp* males but decreased Ma.Ar in 20-week *Hyp* males, 12-week *Hyp* females, and 20-week *Hyp* females. Scl-Ab treatment decreased Ma.Ar in WT animals of both ages and sexes. The 12-week males and 20-week females had significant genotype x treatment interaction for Ma.Ar. The 12-week WT males had a larger decrease in Ma.Ar with Scl-Ab treatment while the 12-week *Hyp* males had a smaller increase in Ma.Ar with treatment (12-week males: 15% decrease in WT, 5% increase in *Hyp*). The 20-week WT females had a larger decrease in Ma.Ar with Scl-Ab treatment compared to the 20-week *Hyp* females (20-week females: 24% WT, 3% *Hyp*).*Hyp* mice had decreased cortical thickness (Ct.Th) compared to WTs in both sexes and age groups. Scl-Ab increased Ct.Th in both sexes and both age groups. Both sexes and age groups had significant

genotype x treatment interaction for Ct.Th with *Hyp* mice having greater relative increases in response to Scl-Ab in the 12-week male group, consistent with the increased Ma.Ar measurement, and WTs having a greater increase in the 12-week female, 20-week male, and 20-week female groups (12-week males: 33% WT, 42% *Hyp*; 12-week females: 31% WT, 30% *Hyp*; 20-week males: 44% WT, 13% *Hyp*; 20-week females: 46% WT, 9% *Hyp*). *Hyp* mice had increased cortical porosity (Ct.Po) when compared to WTs in all groups, but the only significant treatment effect was noted in the 20 week old male group. *Hyp* mice had decreased cortical tissue mineral density (Ct.TMD) compared to WTs in both the 12-week and 20-week old male groups. The 20-week females had significant genotype x treatment interaction for Ct.TMD with WTs having a greater increase in Ct.TMD with Scl-Ab treatment (7% increase WT, 1% decrease in *Hyp*, Supplemental tables 3–6).

Hyp mice in both sexes and age groups also had decreased trabecular bone volume fraction (BV/TV) compared to WTs (Figure 3C and Figure 3D). In both sexes and age groups Scl-Ab treatment increased trabecular bone volume fraction. All groups had significant genotype x treatment interactions for trabecular bone volume fraction. The 12-week male *Hyp* mice had a greater increase in bone volume fraction with Scl-Ab treatment compared to WTs (12-week males: 110% WT, 185% *Hyp*). For all other groups, WTs had a greater increase in bone volume fraction with Scl-Ab treatment compared to *Hyp* mice (12-week females: 259% WT, 10% *Hyp*; 20-week males: 229% WT, 125% *Hyp*: 20-week females: 553% WT, 23% *Hyp*).

Hyp mice had decreased trabecular number (Tb.N) compared to WTs in all groups. Scl-Ab treatment increased Tb.N in the 12-week male, 20-week male, and 20-week female groups. The 12-week female, 20-week male, and 20-week female groups had significant genotype x treatment interaction for Tb.N. The 20-week male *Hyp* mice had a greater increase in Tb.N with Scl-Ab treatment while the 12-week WT female and 20-week WT female groups had a greater increase in Tb.N with Scl-Ab treatment (12-week females: 31% WT, 23% *Hyp*; 20-week males: 12% WT, 12% *Hyp*; 20-week females: 9% WT, and a slight, ~2% decrease in the *Hyp* mice). *Hyp* mice had increased trabecular spacing (Tb.Sp) compared to WTs in all groups. Scl-Ab treatment decreased Tb.Sp in 12-week and 20-week male mice. 12-week and 20-week-old female groups had significant genotype x treatment interaction for Tb.Sp with 12-week female *Hyp* mice had increased Tb.Sp with Scl-Ab treatment compared to WTs and 20-week female WT mice had increased Tb.Sp with Scl-Ab treatment compared to *Hyp* mice (12-week females: 21% WT, 23% *Hyp*; 20-week females: 7% WT, 2% decrease in the *Hyp* mice). Values for all μCT variables are presented within the supplemental data (Supplemental tables 3–6).

Mechanical Testing

Hyp mice of both sexes and age groups had decreased bending moment when compared to WTs (Figures 4 and 5). Scl-Ab treatment increased the bending moment in both sexes of each age group. All groups had significant genotype x treatment interactions for bending moment. The 12-week male and female *Hyp* mice had a greater increase in bending moment with Scl-Ab treatment compared to WTs (12-week males: 90% WT, 110% *Hyp*; 12-week females: 72% WT, 108% *Hyp*). The 20-week male and female WT mice had a greater

increase in bending moment with Scl-Ab treatment compared to *Hyp* mice (20-week males: 91% WT, 68% *Hyp*; 20-week females: 84% WT, 48% *Hyp*). *Hyp* mice of both sexes and age groups had decreased rigidity when compared to WTs. Scl-Ab treatment increased rigidity in both sexes of each age group. All groups had significant genotype x treatment interactions for rigidity. The 12-week male and female *Hyp* mice had a greater increase in rigidity with Scl-Ab treatment compared to WTs (12-week males: 61% WT, 274% *Hyp*; 12-week females: 60% WT, 118% *Hyp*). The 20-week male and female WT mice had a greater increase in rigidity with Scl-Ab treatment compared to *Hyp* mice (20-week males: 59% WT, 42% *Hyp*; 20-week females: 45% WT, 21% *Hyp*).

Skeletal Histology

Dynamic histomorphometry: Bone formation indices were generally lowered in the *Hyp* mice when compared to WTs (Tables 1–4). Scl-Ab treatment significantly increased Tb.MS/BS in both sexes and age groups. The 20-week males and females had a significant genotype x treatment interactions for Tb.MS/BS with WT mice responding to Scl-Ab with a greater increase in Tb.MS/BS when compared to *Hyp* mice (20-week males: 175% WT, 123% *Hyp*; 20-week females: 104% WT, 83% *Hyp).* Scl-Ab treatment significantly increased Tb.MAR in the 12-week males, with *Hyp* mice responding to Scl-Ab with a greater increase in Tb.MAR when compared to WT mice (12-week males: 35% WT, 507% *Hyp*). Scl-Ab significantly increased Tb.BFR in both sexes and age groups. The 12-week female, 20-week male, and 20-week female groups had significant genotype x treatment interactions for Tb.BFR with *Hyp* mice responding to Scl-Ab with a greater increase in Tb.BFR in the 20 week groups (12-week females: 140% WT, 137% *Hyp*; 20-week males: 214% WT, 605% *Hyp*; 20-week females: 81% WT, 657% *Hyp*). Scl-Ab treatment significantly increased Tb.MLT in 12-week-old males only. Scl-Ab treatment significantly increased Ec.MS/BS in the 12-week and 20-week-old females. The 12-week female group had significant genotype x treatment interaction for Ec.MS/BS with WT mice responding to Scl-Ab with a greater increase in Ec.MS/BS (82% WT, 42% *Hyp*). Scl-Ab treatment significantly increased Ec.BFR in the 12-week-old females, but no significant effects were noted in the other groups.

Osteoid: Trabecular osteoid thickness (Tb.O.Th) was decreased in the 12-week female *Hyp* mice compared to WTs (Tables 5–8). There were no Scl-Ab treatment effects on Tb.O.Th in any of the groups. Trabecular osteoid surface/bone surface (Tb.OS/BS) was increased in the 12-week-old male *Hyp* mice compared to WTs and decreased in the 12-week female *Hyp* mice compared to WTs. There were no Scl-Ab treatment effects on Tb.OS/BS in any of the groups. Endocortical osteoid thickness (Ec.O.Th) was increased in *Hyp* mice of all groups when compared to WTs. There were no Scl-Ab treatment effects on Ec.O.Th in any of the groups. The 20-week female group had significant genotype x treatment interactions for Ec.O.Th with *Hyp* mice responding to Scl-Ab with a greater increase in Ec.O.Th, whereas WTs had a decrease in Ec.O.Th (48% WT, 63% *Hyp*). Endocortical osteoid surface/bone surface (Ec.OS/BS) was increased in *Hyp* mice of all groups when compared to WTs. There were no Scl-Ab treatment effects on Ec.OS/BS in any of the groups.

Gene Expression

Gene expression of sodium-phosphate transporters, *Npt2a* and *Npt2c*, was measured in the kidneys of the 12-week cohort. Renal expression of the *Npt2a* gene was significantly decreased in *Hyp* mice of both sexes when compared to WTs (males: p= 0.004, females: p= 0.024). Renal expression of the *Npt2c* gene was also significantly decreased in *Hyp* mice of both sexes when compared to WTs (males: p= 0.045, females: p< 0.001). There was no significant Scl-Ab treatment effect in either sex (Figure 6).

Immunohistochemistry

Renal protein expression of NPT2a was examined using immunostaining (Figure 7 & 8). NPT2a expression was markedly decreased in female vehicle treated *Hyp* mice when compared to WT females. However, the same reduction in NTP2a was not apparent in the male *Hyp* mice. The Scl-Ab treatment response also appears to be sex-dependent, as Scl-Ab treatment of female *Hyp* mice led to increased NTP2a staining, the same change was not present in the Scl-Ab treated male *Hyp* mice.

Discussion

The current study used the adult *Hyp* mouse model to assess the efficacy of Scl-Ab treatment in XLH-related skeletal and metabolic pathologies. Scl-Ab treatment significantly lowered iFGF23 and cFGF23 and improved PTH and vitamin 1,25(OH)2D. Similar to the effects of Scl-Ab in other disease models, there was a significant increase in bone mass and strength and increased bone formation rates in treated *Hyp* mice. While Scl-Ab did not significantly affect the renal gene expression of *Npt2a*, protein expression appeared to increase with Scl-Ab treatment, at least in the female *Hyp* mice. These results suggest that Scl-Ab is capable of rescuing some of the disease pathologies associated with XLH at a later stage in life and support our previous findings in younger *Hyp* mice that sclerostin has a role in phosphate metabolism.

XLH is most commonly diagnosed early in childhood, but the disease is lifelong and progressive. Adult XLH patients commonly suffer from bone pain [6, 20–22] and increased fracture risk [6, 21] due to persistent osteomalacia. The goals for treatment of adult XLH patients are generally targeted at reducing the osteomalacia burden to prevent future fractures [6]. Similar to our previous study in young, growing *Hyp* mice [11], we demonstrated that Scl-Ab treatment significantly increased bone strength, a surrogate measure of fracture risk in murine studies. The increased bone strength was coincident with increase in bone mass and bone formation rate (BFR). Surprisingly, however, the cortical porosity and tissue mineral density parameters were largely unchanged with sclerostin antibody treatment. Therefore, it seems that the increases in bone strength are largely attributed to increased bone size rather than significant improvements in bone quality.

Although bone strength increased with Scl-Ab treatment in both genotypes, the anabolic response to Scl-Ab appeared to differ in wildtype and *Hyp* mice. For example, WT mice increased overall bone size with Scl-Ab treatment, as evident by increased total area and decreased medullary area, whereas *Hyp* mice increased total area but the marrow

area was largely unchanged or saw slight increases with treatment. Periosteal expansion appears to occur naturally in *Hyp* mice, which has been suggested to be a mechanical compensatory reaction to maximize bone strength despite the overall smaller bone size [23]. Therefore, it is likely that the greater response in the periosteal compartment is similarly mechanically advantageous to the *Hyp* skeleton. Sclerostin antibody primarily activates otherwise quiescent lining cells rather than promoting cellular proliferation [24], therefore future work is needed to determine whether the bone lining cell density differs in the endocortical and periosteal surfaces in *Hyp* mice.

The regulation of phosphate metabolism is complex and involves interrelated contributions from FGF23, vitamin 1,25(OH)2D, and PTH [25–27]. Low vitamin 1,25(OH)2D levels and hyperparathyroidism, or high PTH levels, are additional biochemical indications clinically noted in XLH patients [10]. While the hormone levels were not nearly as affected in the *Hyp* mouse model as noted clinically, we found that Scl-Ab significantly increased vitamin 1,25(OH)2D in the 20-week age group. FGF23 is known to decrease vitamin 1,25(OH)2D through regulation of Cyp24A1 and Cyp27B1 [5]. Therefore, the increase in vitamin 1,25(OH)2D with Scl-Ab treatment is potentially secondary to the decrease in circulating FGF23. This is further supported by the findings that sclerostin knock-out mice have elevated vitamin 1,25(OH)2D and decreased FGF23 [12]. However, treatment of cultured proximal tubule cells with sclerostin decreases Cyp27B1 mRNA [12], suggesting that sclerostin may directly affect gene expression.

There was a downward trend in PTH with Scl-Ab treatment in all groups that was significant in the 20-week male group. PTH has previously been found to influence both FGF23 and sclerostin. For example, *in vitro* and *in vivo* studies have shown that PTH increases FGF23 expression in cultured osteocyte-like cells [13, 28–30]. A recent study done in IDG-SW3 osteocyte-like cells found that both sclerostin and PTH treatment increased *Fgf23* mRNA levels [13]. Our study shows that neutralizing sclerostin activity with systemic injection of a sclerostin targeting antibody decreases circulating PTH and FGF23, further supporting a role for sclerostin in the regulation of FGF23.

Renal phosphate wasting in XLH is driven by FGF23 targeted suppression of the sodium-phosphate cotransporters [31]. Our initial study in growing *Hyp* mice found that *Hyp* mice had reduced *Npt2a* expression when compared to WT littermates [11], which is also noted in the adult *Hyp* mice in this study. Additionally, we previously reported that Scl-Ab had no effect on the renal expression of the *Npt2a* gene [11], a finding that we recapitulate in the current study. Immunohistochemistry analyses did reveal an improvement of NPT2a protein expression with Scl-Ab treatment in 20-week-old *Hyp* mice kidneys, which was primarily present in female *Hyp* mice. One potential explanation for this discrepancy is that gene expression was done in total kidney rather than, isolating the proximal tubules, which are the primary source of NPT2a expression. Further, NPT2a is regulated via transcription, translation, and degradation via endocytosis [32–34], therefore sclerostin may be regulating NPT2a through protein translation or degradation mechanisms rather via gene expression. However, the explanation for why the results appear to be sex dependent is currently unclear.

Our previous study investigated growing *Hyp* mice to reflect the clinical reality that XLH is generally first diagnosed in children. In the current study, we investigated mice that were approaching or beyond longitudinal skeletal growth, which is generally noted to plateau around 12 weeks of age in C57 mice [15]. The findings demonstrate that Scl-Ab treatment suppresses FGF23 (iFGF23 and cFGF23), increases bone mass, and improves bone strength. Similar to our previous study in growing *Hyp* mice, male mice generally respond more effectively to Scl-Ab treatment. This may be due to a gene dose effect, as the female *Hyp* mice in this study were heterozygous, while the male mice were hemizygous. However, there is limited data on sex differences in the *Hyp* mouse model and therefore further work is needed to more fully explain the varying treatment response.

The current study has several strengthens, including use of a murine model of XLH that phenocopies and genocopies the majority of clinical XLH pathologies [6], use of an FDA-approved pharmaceutical [35] with the potential for rapid clinical use in XLH patients, and a detailed investigation of the skeletal and metabolic effects of Scl-Ab in the *Hyp* model. Burosumab (anti-FGF23 antibody) is an effective treatment currently used to treat patients with XLH, but our study points to another possible treatment option for XLH. A limitation of this study is that the mechanism responsible for decreasing FGF23 via sclerostin suppression remains unclear. Previous studies suggests that sclerostin increases FGF23 through NFκB signaling or Wnt-signaling [13, 36], but more research is needed to confirm that neutralizing sclerostin activity via Scl-Ab works through the same mechanism and that this remains true in the *Hyp* mice model. The current study suggests that the effects of Scl-Ab on phosphate metabolism is likely through the combined effects on FGF23, PTH, and Vitamin D. However, these combined hormonal changes did not increase circulating phosphate levels, nor was hypophosphatemia evident in the *Hyp* mice despite the highly elevated FGF23 levels. It is unclear why phosphate levels were not reduced in the *Hyp* mice, but it is worth noting that the blood samples were collected in a non-fasting state and the mice received a relatively high phosphate diet (0.7% phosphorus). Additionally, while all terminations occurred at roughly the same time in the afternoon, it is possible that the high circadian fluctuation associated with serum phosphate [37] and renal phosphate excretion [38] are contributing to transiently elevated phosphate levels in the *Hyp* mice.

This study suggests that Scl-Ab treatment can effectively improve many of the skeletal and metabolic pathologies associated with adult XLH patients, further establishes the role of sclerostin in the regulation of FGF23, and provides evidence that Scl-Ab can improve phosphate regulation by targeting the bone-renal axis.

Supplementary Material

Refer to Web version on PubMed Central for supplementary material.

Acknowledgements

Micro-computed tomography scanning was performed within the Rush microCT/histology core facility. Research reported in this publication was supported by the National Institute of Arthritis and Musculoskeletal and Skin Diseases of the National Institute of Health under award no. K01AR073923. The content is solely the responsibility of the authors and does not necessarily represent the official views of the National Institutes of Health. Sclerostin antibody was provided by Amgen Inc, Thousand Oaks, CA, USA, and UCB Pharma, Brussels, Belgium.

References

1. Alon, U.S., Hypophosphatemic vitamin D-resistant rickets. Primer on the Metabolic Bone Diseases and Disorders of Mineral Metabolism, ed. Favus MJ. Vol. 6th Ed. 2006, Washington, DC, USA: The American Society for Bone and Mineral Research. 342–345.
2. A gene (PEX) with homologies to endopeptidases is mutated in patients with X-linked hypophosphatemic rickets. The HYP Consortium. Nat Genet, 1995. 11(2): p. 130–6. [PubMed: 7550339]
3. Pavone V, et al. , Hypophosphatemic rickets: etiology, clinical features and treatment. Eur J Orthop Surg Traumatol, 2015. 25(2): p. 221–6. [PubMed: 24957364]
4. Bergwitz C and Jüppner H, Regulation of Phosphate Homeostasis by PTH, Vitamin D, and FGF23. Annual Review of Medicine, 2010. 61(1): p. 91–104.
5. Shimada T, et al. , FGF-23 Is a Potent Regulator of Vitamin D Metabolism and Phosphate Homeostasis. Journal of Bone and Mineral Research, 2004. 19(3): p. 429–435. [PubMed: 15040831]
6. Carpenter TO, et al. , A clinician's guide to X-linked hypophosphatemia. J Bone Miner Res, 2011. 26(7): p. 1381–8. [PubMed: 21538511]
7. Ben-Dov IZ, et al. , The parathyroid is a target organ for FGF23 in rats. The Journal of Clinical Investigation, 2007. 117(12): p. 4003–4008. [PubMed: 17992255]
8. Krajisnik T, et al. , Fibroblast growth factor-23 regulates parathyroid hormone and 1α-hydroxylase expression in cultured bovine parathyroid cells. Journal of Endocrinology, 2007. 195(1): p. 125–131.
9. Mace ML, et al. , Fibroblast Growth Factor (FGF) 23 Regulates the Plasma Levels of Parathyroid Hormone In Vivo Through the FGF Receptor in Normocalcemia, But Not in Hypocalcemia. Calcified Tissue International, 2018. 102(1): p. 85–92. [PubMed: 29063159]
10. Lecoq A-L, et al. , Hyperparathyroidism in Patients With X-Linked Hypophosphatemia. Journal of Bone and Mineral Research, 2020. 35(7): p. 1263–1273. [PubMed: 32101626]
11. Carpenter KA and Ross RD, Sclerostin Antibody Treatment Increases Bone Mass and Normalizes Circulating Phosphate Levels in Growing Hyp Mice. J Bone Miner Res, 2020. 35(3): p. 596–607. [PubMed: 31743490]
12. Ryan ZC, et al. , Sclerostin alters serum vitamin D metabolite and fibroblast growth factor 23 concentrations and the urinary excretion of calcium. Proc.Natl.Acad.Sci.U.S.A, 2013. 110(15): p. 6199–6204. [PubMed: 23530237]
13. Ito N, et al. , Sclerostin Directly Stimulates Osteocyte Synthesis of Fibroblast Growth Factor-23. Calcified Tissue International, 2021.
14. Bellido T, Saini V, and Pajevic PD, Effects of PTH on osteocyte function. Bone, 2013. 54(2): p. 250–257. [PubMed: 23017659]
15. Glatt V, et al. , Age-related changes in trabecular architecture differ in female and male C57BL/6J mice. J Bone Miner Res, 2007. 22(8): p. 1197–207. [PubMed: 17488199]
16. Ren Y, et al. , Sclerostin antibody (Scl-Ab) improves osteomalacia phenotype in dentin matrix protein 1(Dmp1) knockout mice with little impact on serum levels of phosphorus and FGF23. Matrix Biol, 2016. 52–54: p. 151–161.
17. Bouxsein ML, et al. , Guidelines for assessment of bone microstructure in rodents using micro-computed tomography. Journal of Bone and Mineral Research, 2010. 25(7): p. 1468–1486. [PubMed: 20533309]
18. Jepsen KJ, et al. , Establishing biomechanical mechanisms in mouse models: practical guidelines for systematically evaluating phenotypic changes in the diaphyses of long bones. J Bone Miner Res, 2015. 30(6): p. 951–66. [PubMed: 25917136]
19. Dempster DW, et al. , Standardized nomenclature, symbols, and units for bone histomorphometry: A 2012 update of the report of the ASBMR Histomorphometry Nomenclature Committee. J.Bone Miner.Res, 2013. 28(1): p. 2–17. [PubMed: 23197339]
20. Reid IR, et al. , X-Linked Hypophosphatemia: A Clinical, Biochemical, and Histopathologic Assessment of Morbidity in Adults. Medicine, 1989. 68(6).

21. Skrinar A, et al. , The Lifelong Impact of X-Linked Hypophosphatemia: Results From a Burden of Disease Survey. Journal of the Endocrine Society, 2019. 3(7): p. 1321–1334. [PubMed: 31259293]
22. Carpenter TO, et al. , Burosumab Therapy in Children with X-Linked Hypophosphatemia. N Engl J Med, 2018. 378(21): p. 1987–1998. [PubMed: 29791829]
23. Camacho NP, et al. , Effect of abnormal mineralization on the mechanical behavior of x-linked hypophosphatemic mice femora. Bone, 1995. 17(3): p. 271–278. [PubMed: 8541141]
24. Kim SW, et al. , Sclerostin Antibody Administration Converts Bone Lining Cells Into Active Osteoblasts. J Bone Miner Res, 2017. 32(5): p. 892–901. [PubMed: 27862326]
25. Fukumoto S, Phosphate metabolism and vitamin D. BoneKEy reports, 2014. 3: p. 497–497. [PubMed: 24605214]
26. Saito T and Fukumoto S, Fibroblast Growth Factor 23 (FGF23) and Disorders of Phosphate Metabolism. International journal of pediatric endocrinology, 2009. 2009: p. 496514–496514. [PubMed: 19956747]
27. Choi N-W, Kidney and phosphate metabolism. Electrolyte & blood pressure : E & BP, 2008. 6(2): p. 77–85. [PubMed: 24459526]
28. Kawata T, et al. , Parathyroid Hormone Regulates Fibroblast Growth Factor-23 in a Mouse Model of Primary Hyperparathyroidism. Journal of the American Society of Nephrology, 2007. 18(10): p. 2683–2688. [PubMed: 17855636]
29. Lavi-Moshayoff V, et al. , PTH increases FGF23 gene expression and mediates the high-FGF23 levels of experimental kidney failure: a bone parathyroid feedback loop. American Journal of Physiology-Renal Physiology, 2010. 299(4): p. F882–F889. [PubMed: 20685823]
30. Rhee Y, et al. , Parathyroid hormone receptor signaling in osteocytes increases the expression of fibroblast growth factor-23 in vitro and in vivo. Bone, 2011. 49(4): p. 636–643. [PubMed: 21726676]
31. Tenenhouse HS, et al. , Differential effects of Npt2a gene ablation and X-linked Hyp mutation on renal expression of Npt2c. American Journal of Physiology-Renal Physiology, 2003. 285(6): p. F1271–F1278. [PubMed: 12952859]
32. Biber J, et al. , Regulation of phosphate transport in proximal tubules. Pflügers Archiv - European Journal of Physiology, 2009. 458(1): p. 39–52. [PubMed: 18758808]
33. Hernando N, Gagnon K, and Lederer E, Phosphate Transport in Epithelial and Nonepithelial Tissue. Physiological Reviews, 2021. 101(1): p. 1–35. [PubMed: 32353243]
34. Kaneko I, et al., Chapter 36 - Transcriptional Regulation of Sodium-Phosphate Cotransporter Gene Expression, in Molecular, Genetic, and Nutritional Aspects of Major and Trace Minerals, Collins JF, Editor. 2017, Academic Press: Boston. p. 437–445.
35. Cosman F, et al. , Romosozumab Treatment in Postmenopausal Women with Osteoporosis. N Engl J Med, 2016. 375(16): p. 1532–1543. [PubMed: 27641143]
36. Liu S, et al. , Novel regulators of Fgf23 expression and mineralization in Hyp bone. Mol Endocrinol, 2009. 23(9): p. 1505–18. [PubMed: 19556340]
37. Portale AA, Halloran BP, and Morris RC Jr., Dietary intake of phosphorus modulates the circadian rhythm in serum concentration of phosphorus. Implications for the renal production of 1,25-dihydroxyvitamin D. The Journal of clinical investigation, 1987. 80(4): p. 1147–1154. [PubMed: 3654974]
38. Stow LR and Gumz ML, The circadian clock in the kidney. Journal of the American Society of Nephrology : JASN, 2011. 22(4): p. 598–604. [PubMed: 21436284]

Highlights:

- Sclerostin antibody treatment decreases circulating fibroblast growth factor-23, increases vitamin 1,25(OH)2D, and decreases parathyroid hormone in adult *Hyp* mice.
- Sclerostin antibody treatment increases bone mass, bone formation rate, and bone strength in adult *Hyp* mice.
- Sclerostin antibody treatment increases NPT2a protein expression, particularly in female Hyp mice.

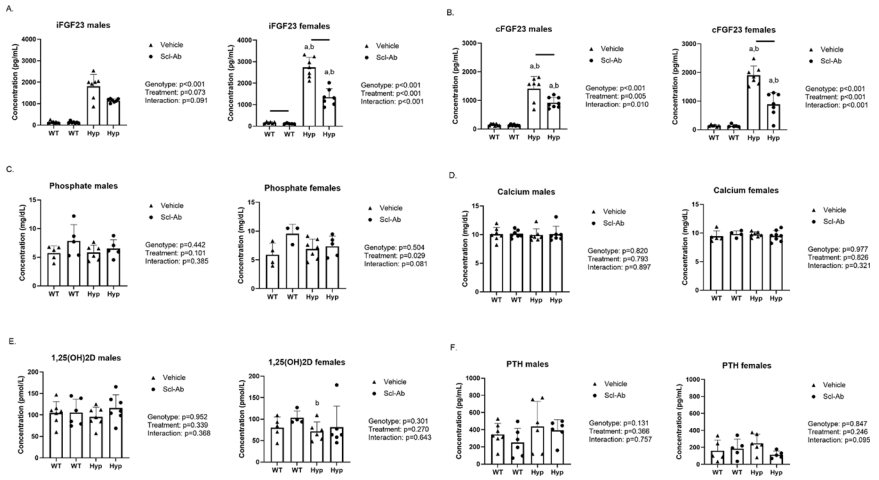

Figure 1.

Mineral metabolism markers for 12-week-old male and female mice; intact FGF23 (A), c-term FGF23 (B), phosphate (C), calcium (D), 1,25(OH)2D (E), and PTH (F). Data are presented as the mean ± standard deviation. Results from the two-way ANOVA are presented in the figure legends. Significant post-hoc differences are reported above the data, with horizontal bars highlighting significant treatment differences between animals of the same genotype and letters highlighting significant differences between *Hyp* mice and vehicle treated WTs (a) and Scl-Ab treated WTs (b).

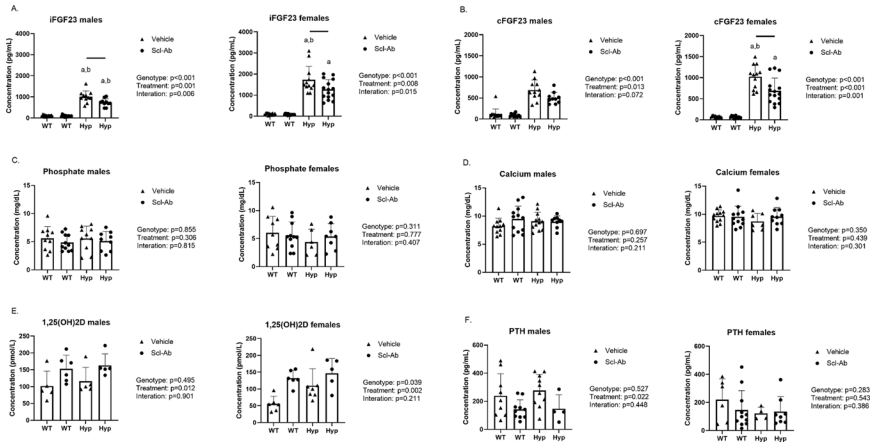

Figure 2.

Mineral metabolism markers for 20-week-old male and female mice; intact FGF23 (A), c-term FGF23 (B), phosphate (C), calcium (D), 1,25(OH)2D (E), and PTH (F). Data are presented as the mean ± standard deviation. Results from the two-way ANOVA are presented in the figure legends. Significant post-hoc differences are reported above the data, with horizontal bars highlighting significant treatment differences between animals of the same genotype and letters highlighting significant differences between *Hyp* mice and vehicle treated WTs (a) and Scl-Ab treated WTs (b).

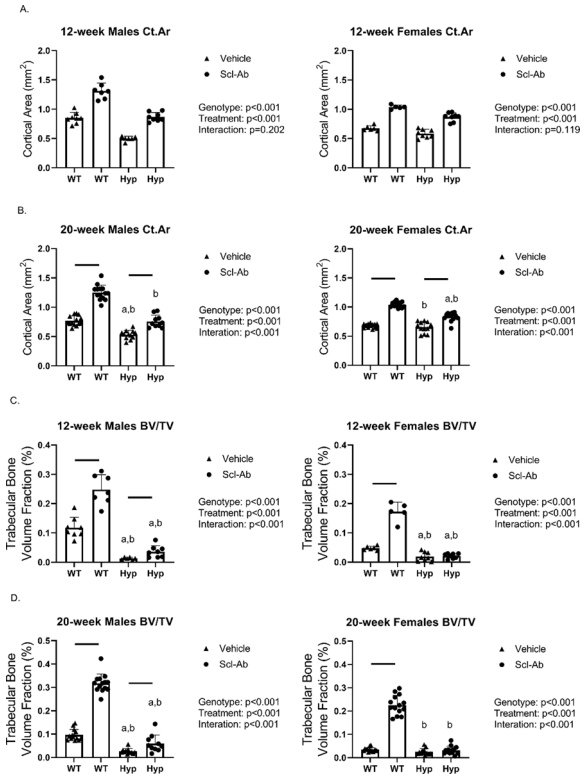

Figure 3.

μCT data of cortical area (Ct.Ar) (A & B) and bone volume/total volume (BV/TV) (C & D) in 12 and 20-week-old mice. Data from male mice are presented on the left and female mice data are on the right. Data are presented as the mean ± standard deviation. Results from the two-way ANOVA are presented in the figure legends. Significant post-hoc differences are reported above the data, with horizontal bars highlighting significant treatment differences between animals of the same genotype and letters highlighting significant differences between *Hyp* mice and vehicle treated WTs (a) and Scl-Ab treated WTs (b).

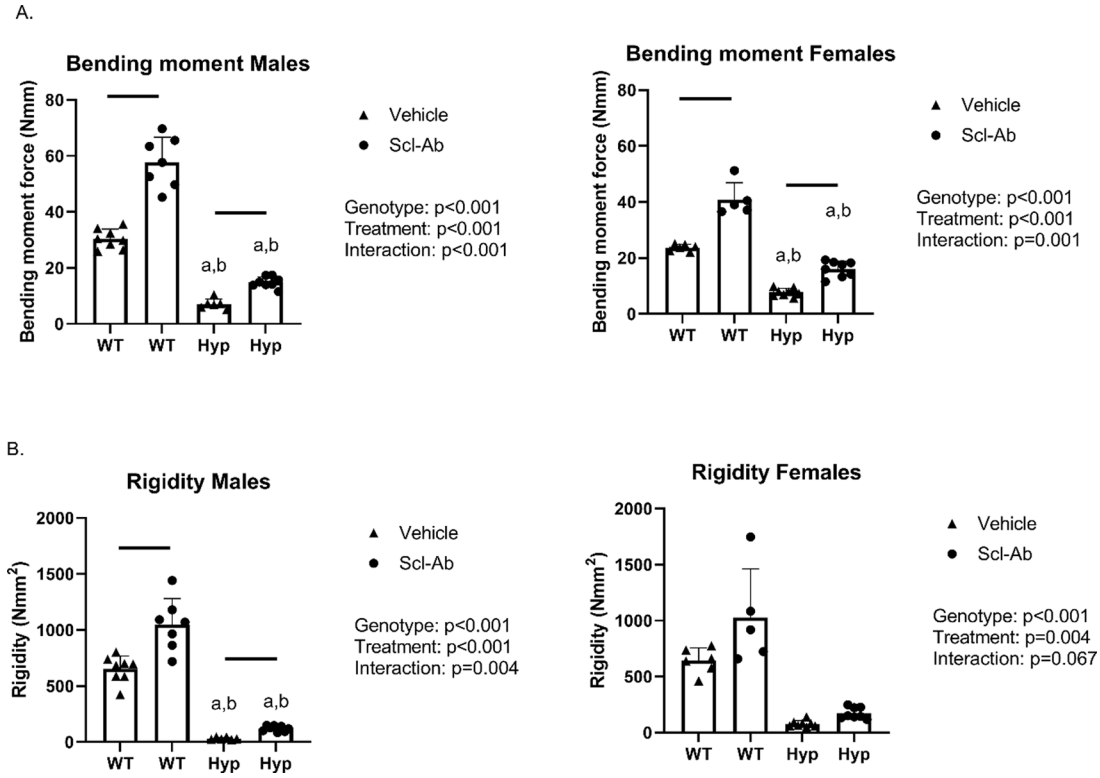

Figure 4.

Mechanical data of bending moment (A) and rigidity (B) in the 12-week-old mice. Data from male mice are presented on the left and female mice data are on the right. Data are presented as the mean ± standard deviation. Results from the two-way ANOVA are presented in the figure legends. Significant post-hoc differences are reported above the data, with horizontal bars highlighting significant treatment differences between animals of the same genotype and letters highlighting significant differences between *Hyp* mice and vehicle treated WTs (a) and Scl-Ab treated WTs (b).

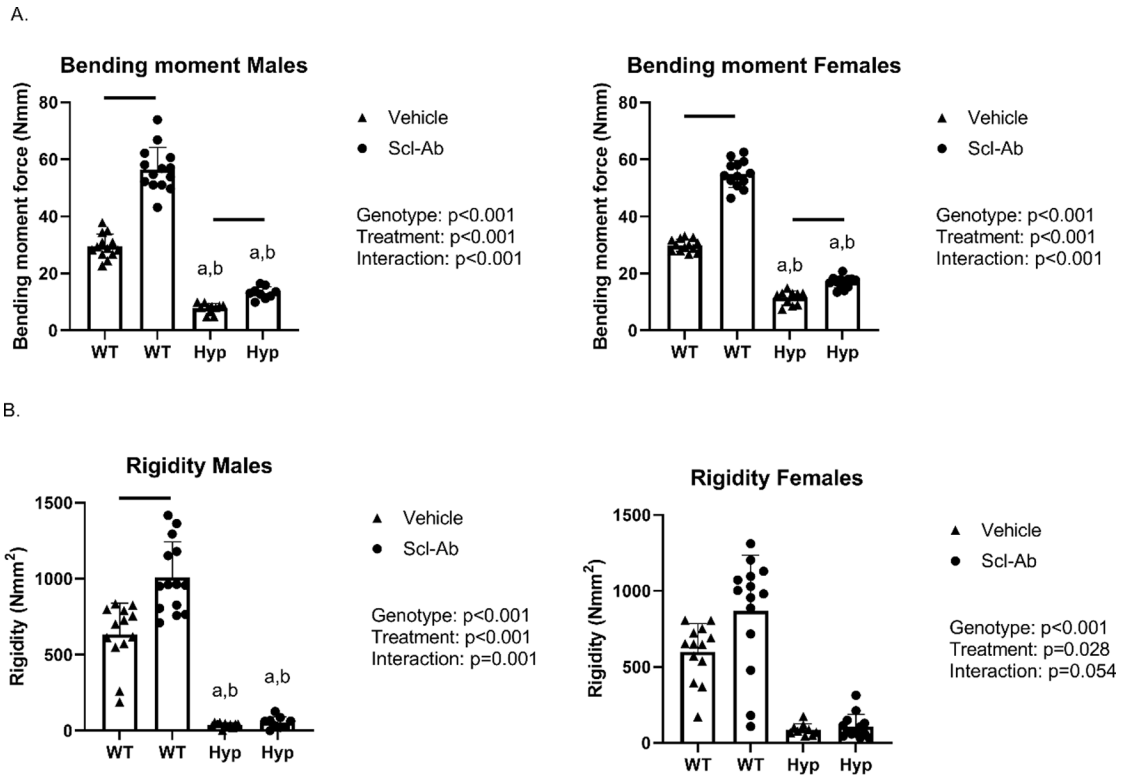

Figure 5.

Mechanical data of bending moment (A) and rigidity (B) in the 20-week-old mice. Data from male mice are presented on the left and female mice data are on the right. Data are presented as the mean ± standard deviation. Results from the two-way ANOVA are presented in the figure legends. Significant post-hoc differences are reported above the data, with horizontal bars highlighting significant treatment differences between animals of the same genotype and letters highlighting significant differences between *Hyp* mice and vehicle treated WTs (a) and Scl-Ab treated WTs (b).

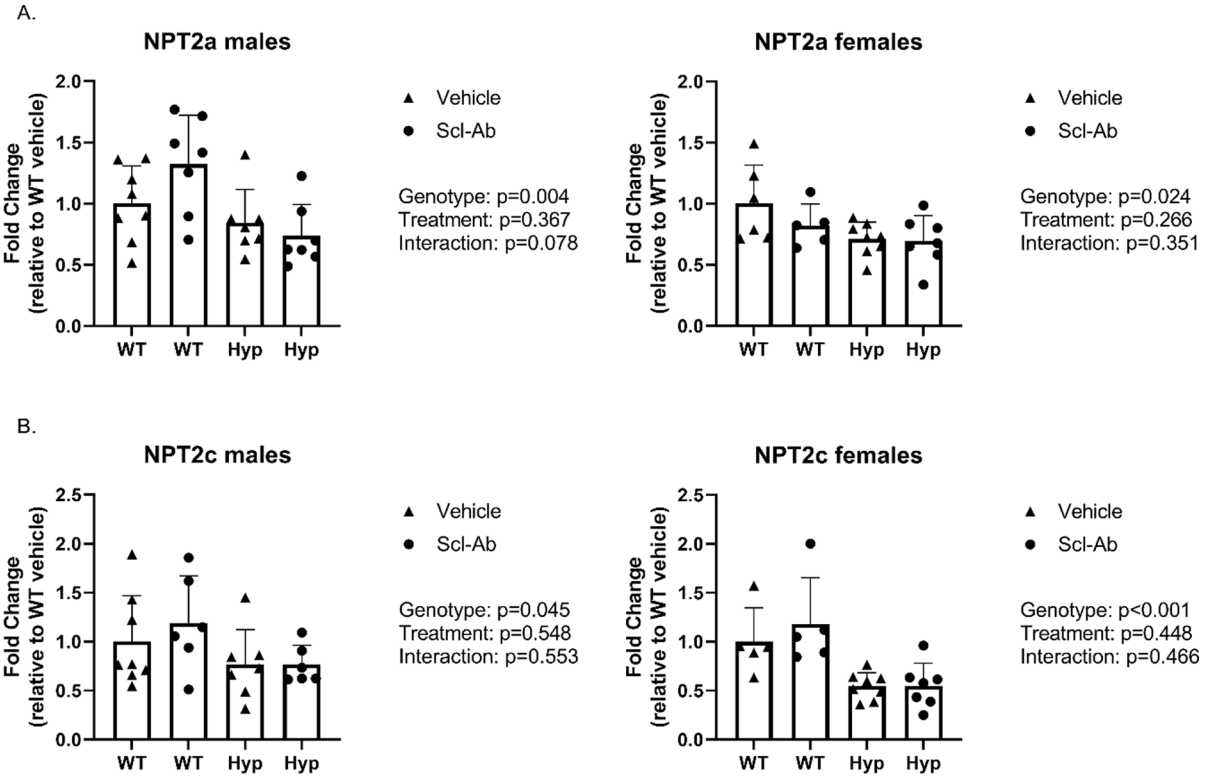

Figure 6.

Gene expression data of kidney sodium-phosphate transporters NPT2a (A) and NPT2c (B) in the 12-week-old mice. Data from male mice are presented on the left and female mice data are on the right. Data are presented as the mean ± standard deviation. Results from the two-way ANOVA are presented in the figure legends.

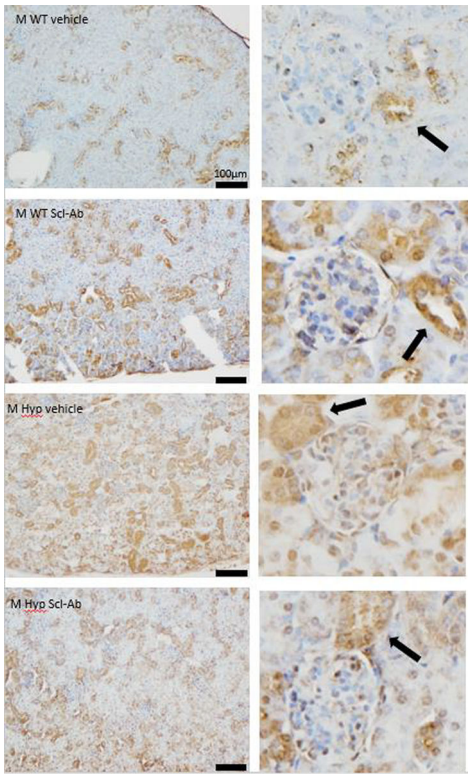

Figure 7.

Representative NPT2a immunohistochemistry kidney sections from 20-week-old male mice. Left panels are representative images at 10x, while right panels are insets at 20x highlighting the glomeruli and proximal tubules. The black arrows point to the proximal tubules the primary location of NPT2a expression. Scale bar = 100μm.

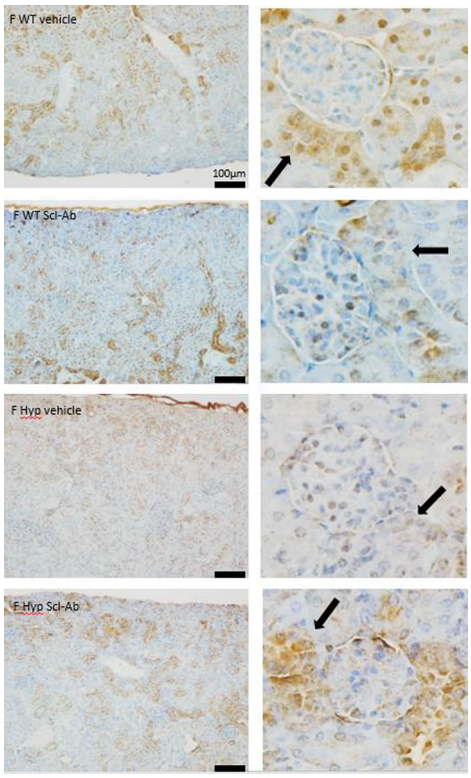

Figure 8.

Representative NPT2a immunohistochemistry kidney sections from 20-week-old female mice. Left panels are representative images at 10x, while right panels are insets at 20x highlighting glomeruli and proximal tubules. The black arrows point to the proximal tubules, the primary location of NPT2a expression. Scale bar = 100μm.

Table 1.

Dynamic Histology results for 12-week-old males of each genotype and treatment group.

	Male WT vehicle	Male WT Scl-Ab	Male Hyp vehicle	Male Hyp Scl-Ab	Genotype effect	Treatment effect	Interaction term
Tb.MS/BS	16.28 ± 3.94	27.62 ± 3.36	3.98 ± 2.71	19.39 ± 9.06	**<0.001**	**<0.001**	0.374
Tb.MAR	1.32 ± 0.19	1.78 ± 0.25[1]	0.30± 0.00[2,3]	1.82 ± 0.44[1,2]	**<0.001**	**<0.001**	**<0.001**
Tb.BFR	78.90 ± 25.26	180.32 ± 41.23	2.98 ± 3.30	128.44 ± 61.92	**0.001**	**<0.001**	0.478
Tb.MLT	0.37 ± 0.67	1.67 ±2.41	undetected	6.39 ± 5.07	**0.089**	**0.005**	0.490
Ec.MS/BS	48.82 ± 14.44	50.74 ± 10.82	19.54 ± 3.28	24.34 ± 8.70	**<0.001**	0.463	0.752
Ec.MAR	2.06 ± 0.14	2.10 ± 0.20	1.22 ± 0.99	1.83 ± 0.61	**0.034**	0.188	0.245
Ec.BFR	365.41 ± 102.78	390.79 ± 107.16	95.66 ± 91.86	173.24 ± 102.54	**<0.001**	0.252	0.556
Ec.MLT	2.89 ± 0.57	1.43 ± 1.45	37.29 ± 51.68	18.31 ± 8.09	**0.034**	0.370	0.441

Data are presented as the mean ± standard deviation. Results from the two-way ANOVA are also presented with statistically significant p-values bolded. Significant post hoc differences are reported as superscripts

[1] indicates significant differences between vehicle and Scl-Ab-treated mice of the same genotype

[2] indicates significant differences from vehicle-treated WT mice

[3] indicates significant differences from Scl-Ab-treated WT mice.

Table 2.

Dynamic Histology results for 12-week-old females of each genotype and treatment group.

	Female WT vehicle	Female WT Scl-Ab	Female Hyp vehicle	Female Hyp Scl-Ab	Genotype effect	Treatment effect	Interaction term
Tb.MS/BS	16.21 ± 1.66	35.54 ± 5.46	09.11 ± 7.55	15.85 ± 11.40	**0.001**	**0.001**	0.069
Tb.MAR	1.83± 0.48	2.00 ± 0.29	0.66 ± 0.74	0.69± 0.56	**<0.001**	0.679	0.764
Tb.BFR	107.11 ± 26.23	257.18 ± 36.79[1]	23.59 ± 27.68[2,3]	55.90 ± 71.35[3]	**<0.001**	**<0.001**	**0.007**
Tb.MLT	2.02 ± 2.48	0.94 ± 1.32	undetected	undetected	**0.034**	0.407	0.407
Ec.MS/BS	37.33± 12.27	68.03 ± 5.88[1]	18.94 ± 11.75[2,3]	26.92 ± 8.70[3]	**<0.001**	**<0.001**	**0.020**
Ec.MAR	2.74 ± 1.06	2.65 ± 0.42	1.04 ± 0.61	1.82 ± 0.42	**0.001**	0.262	0.159
Ec.BFR	408.54± 252.34	655.10 ± 100.17	90.90 ± 75.78	184.52 ± 82.17	**<0.001**	**0.015**	0.240
Ec.MLT	2.69 ± 1.71	1.88 ± 1.27	47.36 ± 46.41	11.65 ± 4.46	**0.034**	0.140	0.158

Data are presented as the mean ± standard deviation. Results from the two-way ANOVA are also presented with statistically significant p-values bolded. Significant post hoc differences are reported as superscripts

[1]indicates significant differences between vehicle and Scl-Ab-treated mice of the same genotype

[2]indicates significant differences from vehicle-treated WT mice

[3]indicates significant differences from Scl-Ab-treated WT mice.

Table 3.

Dynamic Histology results for 20-week-old males of each genotype and treatment group.

	Male WT vehicle	Male WT Scl-Ab	Male Hyp vehicle	Male Hyp Scl-Ab	Genotype effect	Treatment effect	Interaction term
Tb.MS/BS	6.18 ± 2.01	17.02 ± 6.45[1]	0.30± 0.00[2,3]	0.67 ± 0.85[2,3]	**<0.001**	**<0.001**	**<0.001**
Tb.MAR	1.15 ± 0.21	1.39 ± 0.09	1.70 ± 2.92	1.53 ± 1.13	0.492	0.999	0.750
Tb.BFR	26.35 ± 11.34	82.87 ± 34.14[1]	1.86 ± 3.21[2,3]	13.12 ± 22.78[3]	**0.001**	**<0.001**	**0.008**
Tb.MLT	undetected	0.37 ±0.91	9.97 ± 7.71	20.26 ± 20.41	0.141	0.869	0.819
Ec.MS/BS	16.15 ± 8.85	19.29 ± 11.47	6.30 ± 3.31	8.66 ± 2.94	**0.001**	0.340	0.900
Ec.MAR	1.41 ± 0.34	1.26 ± 0.11	0.55± 0.942[2,3]	1.53 ± 1.13[1]	0.210	0.080	**0.021**
Ec.BFR	85.23 ± 53.86	87.84 ± 52.02	14.40 ± 14.81	52.72 ± 50.36	**0.005**	0.243	0.307
Ec.MLT	1.50 ± 2.13	2.67 ± 2.98	29.64 ± 25.91	33.79 ± 54.99	**0.025**	0.836	0.909

Data are presented as the mean ± standard deviation. Results from the two-way ANOVA are also presented with statistically significant p-values bolded. Significant post hoc differences are reported as superscripts

[1] indicates significant differences between vehicle and Scl-Ab-treated mice of the same genotype

[2] indicates significant differences from vehicle-treated WT mice

[3] indicates significant differences from Scl-Ab-treated WT mice.

Table 4.

Dynamic Histology results for 20-week-old females of each genotype and treatment group.

	Female WT vehicle	Female WT Scl-Ab	Female Hyp vehicle	Female Hyp Scl-Ab	Genotype effect	Treatment effect	Interaction term
Tb.MS/BS	10.69 ± 4.92	21.87 ± 4.33[1]	0.30 ± 0.00[2,3]	0.55 ± 0.54[2,3]	**<0.001**	**<0.001**	**<0.001**
Tb.MAR	1.75± 0.32	1.69 ± 0.33	2.29 ± 5.36	4.40 ± 7.28	0.286	0.499	0.475
Tb.BFR	74.94 ± 39.51	135.68 ± 39.59[1]	2.51 ± 5.87[2,3]	19.01 ± 37.02[2,3]	**<0.001**	**0.001**	**0.041**
Tb.MLT	0.82 ± 1.54	2.12 ± 1.62	13.05 ± 34.54	0.85 ± 2.56	0.362	0.365	0.264
Ec.MS/BS	28.32 ± 13.71	41.15 ± 13.34	9.85 ± 2.84	14.13 ± 4.11	**<0.001**	**0.008**	0.140
Ec.MAR	1.76 ± 0.62	1.654± 0.25	0.30 ± 0.00	0.65 ± 0.71	**0.001**	0.439	0.176
Ec.BFR	185.70 ± 109.95	246.08 ± 88.57	10.79 ± 3.11	32.91 ± 30.86	**<0.001**	0.063	0.318
Ec.MLT	3.08 ± 2.95	1.68 ± 2.38	42.07 ± 15.38	52.72 ± 26.29	**<0.001**	0.435	0.311

Data are presented as the mean ± standard deviation. Results from the two-way ANOVA are also presented with statistically significant p-values bolded. Significant post hoc differences are reported as superscripts

[1]indicates significant differences between vehicle and Scl-Ab-treated mice of the same genotype

[2]indicates significant differences from vehicle-treated WT mice

[3]indicates significant differences from Scl-Ab-treated WT mice.

Table 5.

Osteoid results for 12-week-old males of each genotype and treatment group.

	Male WT vehicle	Male WT Scl-Ab	Male Hyp vehicle	Male Hyp Scl-Ab	Genotype effect	Treatment effect	Interaction term
Tb.O.Th	0.55 ± 1.07	3.06 ± 4.39	1.99 ± 4.87	8.32 ±7.81	0.137	0.055	0.385
Tb.OS/BS	0.07 ± 0.12	0.06 ± 0.07	8.32 ± 20.38	34.33 ±33.68	**0.021**	0.141	0.140
Ec.O.Th	5.96 ± 1.23	2.82 ± 2.70	23.74 ± 16.27	29.55 ± 12.62	**<0.001**	0.738	0.271
Ec.OS/BS (%)	6.12 ± 7.19	1.04 ± 1.40	82.65 ± 16.47	83.10 ±19.49	**<0.001**	0.692	0.636

Data are presented as the mean ± standard deviation. Results from the two-way ANOVA are also presented with statistically significant p-values bolded. Significant post hoc differences are reported as superscripts

1 indicates significant differences between vehicle and Scl-Ab-treated mice of the same genotype

2 indicates significant differences from vehicle-treated WT mice

3 indicates significant differences from Scl-Ab-treated WT mice.

Table 6.

Osteoid results for 12-week-old females of each genotype and treatment group.

	Female WT vehicle	Female WT Scl-Ab	Female Hyp vehicle	Female Hyp Scl-Ab	Genotype effect	Treatment effect	Interaction term
Tb.O.Th	4.21 ± 5.13	2.06 ± 2.91	0.00 ± 0.00	0.00 ± 0.00	**0.017**	0.380	0.380
Tb.OS/BS	0.94 ± 1.34	1.51 ± 2.5	0.00 ± 0.00	0.00 ± 0.00	**0.047**	0.624	0.624
Ec.O.Th	6.13 ± 1.16	4.79 ± 2.87	25.59 ± 6.66	20.90 ± 5.72	<**0.001**	0.172	0.438
Ec.OS/BS (%)	10.12 ± 6.64	9.99 ± 10.89	88.69 ± 5.21	85.19 ± 18.87	<**0.001**	0.710	0.730

Data are presented as the mean ± standard deviation. Results from the two-way ANOVA are also presented with statistically significant p-values bolded. Significant post hoc differences are reported as superscripts

*1*indicates significant differences between vehicle and Scl-Ab-treated mice of the same genotype

*2*indicates significant differences from vehicle-treated WT mice

*3*indicates significant differences from Scl-Ab-treated WT mice.

Table 7.

Osteoid results for 20-week-old males of each genotype and treatment group.

	Male WT vehicle	Male WT Scl-Ab	Male Hyp vehicle	Male Hyp Scl-Ab	Genotype effect	Treatment effect	Interaction term
Tb.O.Th	0.00 ± 0.00	0.62 ± 1.39	4.36 ± 6.88	2.34 ± 6.10	0.126	0.719	0.497
Tb.OS/BS (%)	0.00 ± 0.00	0.02 ± 0.41	14.97 ± 24.24	2.33 ± 6.15	0.096	0.217	0.216
Ec.O.Th	1.89 ± 2.91	3.85 ± 3.69	15.45 ± 8.8	22.91 ± 11.86	**<0.001**	0.159	0.404
Ec.OS/BS (%)	0.93 ± 1.72	0.46 ± 0.62	39.21 ± 24.36	72.61 ± 38.58	**<0.001**	0.102	0.093

Data are presented as the mean ± standard deviation. Results from the two-way ANOVA are also presented with statistically significant p-values bolded. Significant post hoc differences are reported as superscripts

1 indicates significant differences between vehicle and Scl-Ab-treated mice of the same genotype

2 indicates significant differences from vehicle-treated WT mice

3 indicates significant differences from Scl-Ab-treated WT mice.

Table 8.

Osteoid results for 20-week-old females of each genotype and treatment group.

	Female WT vehicle	Female WT Scl-Ab	Female Hyp vehicle	Female Hyp Scl-Ab	Genotype effect	Treatment effect	Interaction term
Tb.O.Th	1.39 ± 2.44	3.65 ± 2.76	3.91 ± 10.36	1.36 ± 4.31	0.954	0.945	0.244
Tb.OS/BS (%)	0.33 ± 0.57	0.26 ± 0.26	5.47 ± 14.48	8.67 ± 27.44	0.273	0.797	0.789
Ec.O.Th	5.34 ± 4.23	2.77 ± 3.87	12.62 ± 4.62[2,3]	20.61 ± 8.99[2,3]	**<0.001**	0.231	**0.024**
Ec.OS/BS (%)	10.37 ± 20.44	0.76 ± 1.11	56.40 ± 24.53	65.21 ± 33.98	**<0.001**	0.964	0.298

Data are presented as the mean ± standard deviation. Results from the two-way ANOVA are also presented with statistically significant p-values bolded. Significant post hoc differences are reported as superscripts

[1] indicates significant differences between vehicle and Scl-Ab-treated mice of the same genotype

[2] indicates significant differences from vehicle-treated WT mice

[3] indicates significant differences from Scl-Ab-treated WT mice.